Letters in High Energy Physics
ISSN: 2632-2714
Volume 2024

Retrieval of Land Surface Temperature by Utility of the Remote Sensing Techniques from Landsat-9 TIRS-2 Data, A Case Study of the Tigris River in Wasit - Iraq.

Haider Majid Tuma[1], Mutasim Ibrahim Malik[2]

[1,2]Department of Physics, College of Science, Wasit University, Kut, Iraq.

[*]E-mail: hmtuma@uowasit.edu.iq

Abstract

This research proposes the Split-Window (SW) and Mono-Window (MW) algorithms for obtaining Land Surface Temperature (LST) from Landsat- 9 TIRS- 2 data. Given this, there are several chances to research land dynamics using remote sensing techniques thanks to LANDSAT data. Compared to other conventional ways, this one is not only less time-consuming but also far more efficient. It also costs less. The present Tigris River study was carried out in the Wasit region of Iraq, where we measured the LST difference over a $136(\mathrm{km})$ section of the Tigris River in 2024 for both the winter and spring seasons. The land surface emissivity (LSE) determination was carried out with the help of the NDVI threshold value. The spatial distribution of LST for winter using an MW was ($10.926 - 12.357°C$), RMSE of ($1.9526°C$), and the Bias of ($1.9436°\mathrm{C}$), while for spring, it was ($14.589 - 16.7434°\mathrm{C}$), RMSE of ($1.2864°\mathrm{C}$), and the Bias of ($1.2164°C$). The spatial distribution of LST using a SW in winter was ($9.275 - 10.651°C$), RMSE of ($0.4684°\mathrm{C}$), and the Bias ($0.3660°\mathrm{C}$), and in spring, it was ($13.4141 - 15.8087°\mathrm{C}$), RMSE of ($0.5231°\mathrm{C}$), and the Bias of ($0.2259°\mathrm{C}$). The regression study between SW and MW algorithms for LST retrieval shows an R^2 value of 0.844 in winter and an R^2 value of 0.9819 in spring. The results were validated by juxtaposing them with LST measurements taken at the twelve research sites during the satellite picture acquisition for both seasons. In conclusion, the proposed split window algorithm gave very similar results with little difference from the in situ recorded results and is predictable to be an authoritative method for retrieval LST from Landsat-9 TIRS- 2data.

Keywords: Remote Sensing (RS), Land Surface Temperature (LST), Landsat-9 thermal infrared sensor-2 (TIRS-2) data, Split-Window Algorithm (SW), Mono-Window Algorithm (MW).

1. Introduction

Iraq is facing a significant problem, otherwise called climatic change, and the effects of global warming[1]. Land Surface Temperature (LST) is regarded as one of the paramount indices of climate fluctuation on a global scale. It is employed in numerous applications, including hydrological, meteorological, climatological, heat balance research, and vegetation water stress[2]. There is tremendous potential for remote sensing in the fields relating to climatology, hydrology, agriculture, and natural resource management; one of the most important utilization of remote sensing is in estimating the change in Earth's surface temperature[2, 3]. Remote sensing as a technology provides input towards efficient and effective collection of information on Earth's surface temperature, enhancing information on environmental and climate change and enhancing decision-making affecting many important fields. There is a need to use remote sensing methods to evaluate the spatial distribution of stream temperatures of rivers and lakes in a way that correlates with water quality problems [4, 5]. LST is the main agent for computing a location's highest and lowest temperatures. LST is a vital meteorological parameter used to estimate surface soil moisture to a large extent[6, 7], estimate evaporation in crops and transpiration, the temperature of water bodies, the intensity of heat in metropolitan islands, compute surface radiative flux, etc.[8, 9]. Information concerning the long-term features of time-related and regional allocation of LST is highly important for understanding the dynamics of exterior energy and water equilibrium, the patterns of the carbon cycle in the Earth's atmosphere, and the processes of global climate change [10, 11]. Recognizing the current usage, the

International Geosphere-Biosphere-Programme (IGBP) has identified Land Surface Temperature (LST) as very important. LST can be reliably attained by applying thermal infrared remote sensing (RS) techniques to directly determine the radiance level of the thermal infrared radiant energy emitted by the land surface[12-14]. On September 27, 2021, the Landsat program successfully deployed Landsat-9, the most recent addition to the satellite series, extending its continuous fifty-year data collection[15]. Landsat-9 is mostly identical to Landsat-8 since it has two sensors: an operational land imager2 (OLI-2) and a thermal infrared sensor2 (TIRS-2)[16]. Landsat-9 TIRS-2, like the Landsat-8 TIRS-1, has two TIR bands integrated to perform thermal calculations. This sensor is mainly built to feature two side bands for sensing thermal infrared radiation. Namely, band 10 operates in the range of $(9.8\ to\ 11.8\mu m)$ and band 11 in the range $(11\ to\ 13\mu m)$[15, 17, 18]. The retrieval of LST considered the OLI sensor from bands $(2\ to\ 5)$, which were used in estimating the Land Surface Emissivity (LSE), making considerations for the Fractional Vegetation Cover (FVC). Numerous recent research attempts have been made to determine the SW approach to obtaining the Landsat-8 TIR data's LST following wander light correction. The LST retrieval efficiency achieved by these efforts is comparable to that of a single-channel method [19-21]. This study shows the use of the SW in the LST retrieval to utilize its benefits and improve the achievement of its results. Besides, two new features built on physical properties illustrating the land surface and atmospheric conditions have existed and developed. These features, known as When leaving the ground temperature of brightness (TB) and water vapor index (W), were derived from the thermal radiance transfer equation by using the top-of-atmosphere temperature of brightness [15]. Countless research has enhanced the SW approach by incorporating the effects of LSE , viewing zenith angle (VZA), and atmospheric water vapor (W) in the retrieval of LST [16]. Such items have been loaded regarding the coefficients of the SW method. USGS has lately published the analysis-ready data (ARD) LST item, which was advanced from Landsat-9 TIRS-2 data utilizing the operational single-channel approach, after the release of the same product for Landsat-8 TIRS-1[22, 23]. In general, Landsat -9TIRS-2 can be considered a refined model of Landsat -8 TIRS-1 with a solution of two main problems: the failure of the scene selects mirror and the influence of the stray light effect[22]. On the other hand, two contingent TIR bands of Landsat -9TIRS-2 enable the application of the SW method to obtain the LST. The SW technique is the most popular algorithm for obtaining LST utilizing thermal infrared remote sensing (TIR) data. This method works out the distinction in the absorption of atmospheric between two neighboring TIR pathways with a central wavelength of $(10-12\mu m)$[24]. Price was the first to create a SW approach. Since then, other SW approaches have been suggested for LST retrieval[13, 25]. These methods can be categorized into two classes, i.e., linear SW method and nonlinear SW method [16, 26-28]. The linear SW technique is an addition technique that estimates the LST based on the linear combination of the two TIR bands using their brightness temperatures. The SW approach, on the other hand, computes this ratio of brightness temperatures more nonlinearly through the addition of an extra term that is the square of the contrast between the two temperatures of brightness in the linear calculation[13, 16]. Some researchers have expanded the SW approach by including the impact of LSE, which affects the estimation of LST, and by combining these aspects regarding the coefficients of the SW procedure [18, 29, 30]. Moreover, later studies have modified the basic two-channel SW approach and have developed the three-channel and four-channel SW techniques. These researches have shown that three- and four-channel SW methods yield better results than the two-channel method[31]. Nevertheless, the threechannel and fourchannel SW are not the right choices for processing the Landsat-8TIRS-1 data because of the availability of only two thermal bands[32]. As a result, we have developed an extremely precise SW approach for the LST retrieval, and the simplified radiative transfer equation still retains a sizable portion of the experimentally observed Planck function. The mono-window (MW) technique uses data from sensors mounted on satellites or aircraft to compute LST, gathering inforamation from a broad sources range. This covers bands in the thermal infrared (TIR), shortwave infrared (SWIR), and visible and near -infrared(NIR) spectrums. Since surface temperatures are closely related to surface physical features, the normalized difference vegetation index (NDVI) analysis is a perfect method for calculating LST. The application

involves vegetation statistical status estimation utilizing parameters like NDVI [33]. Data like Landsat-9 have a medium spatial resolution, making it good for mapping out land cover, vegetation, or even water cover areas at the local or regional level. Landsat-9 satellite has two devices: an Operational Land Imager2, also known as (OLI-2), and a Thermal Infrared Sensor2, also known as (TIRS-2). OLI-2 gathers data with a ground sampling of 30 meters having eight spectral bands in the visible, nearinfrared, and shortwave infrared portions of the electromagnetic spectrum and an extra highresolution panchromatic band at a ground sampling of 15 meters. TIRS-2 measures TIR radiation with a resolution of spatial of 100 meters and is equipped with two bands ranging from $(10-12\mu m)$, which in this context is known as the Atmospheric Window[17]. There are many scientific disciplines in which LST holds significance. As mentioned earlier, the LST is the thermostat that controls the flow of water and energy between the atmosphere and the Earth's surface. It is, therefore, crucial to use it in the climate change field and during development to assess how changes in land cover affect the temperature of the surface.

2. Description of Study Sites

Tigris River is a major river in Iraq traversing across many governorates and through Wasit governorate (Fig 1). It can be said to be situated at the center of the country. This region is basically a farming area due to the presence of the Tigris River. The research area lies between latitude 32.6111°N to 32.1167°N and a longitude of 45.7611°E to 45.8833°E. The region's elevation is 35 meters higher than the average sea level [34]. Remote sensing can supply proper and uninterrupted data to forecast the surface temperature of the Tigris River in the study area. To validate temperature retrieval over the research area, we sampled 12 stations on the stretch of the river (136 km) (Table 1). The SW and the MW algorithm calculated the thermal condition of the river's surface. We compared it to the temperature obtained at the study site by an infrared thermometer (IR thermometer) synchronized with satellite image capture.

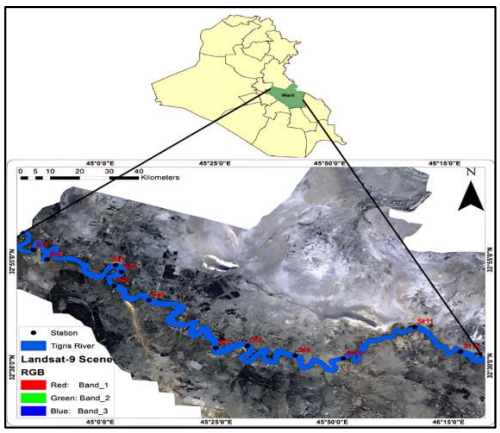

Fig 1. The study area of Wasit District.

Table 1. Location of temperature coordinates.

Station	Coordinates	
	Latitude (N)	Longitude (E)
St1	32°57'56.38"N	44°45'30.94"E
St2	32°55'30.42"N	44°48'26.63"E
St3	32°54'10.15"N	45° 3'21.02"E
St4	32°52'34.77"N	45° 4'36.86"E
St5	32°49'21.65"N	45° 2'58.77"E
St6	32°45'56.39"N	45°10'30.10"E
St7	32°34'55.46"N	45°24'55.74"E
St8	32°35'9.11"N	45°31'49.95"E
St9	32°32'44.10"N	45°42'6.89"E
St10	32°31'54.61"N	45°52'29.40"E
St11	32°39'19.90"N	46° 7'57.48"E
St12	32°33'21.91"N	46°17'49.51"E

3. Methodology of Research

The present study uses the SW and MW algorithm techniques, in which LST extraction is done using data from Landsat-9 Thermal Infrared Sensor, known by the abbreviation TIRS-2. Besides the TIRS-2 data, the SW and MW algorithms also require the data on OLI-2 to compute LST. We should layer the Landsat-9 OLI-2 sensor bands on 2, 3, 4, and 5, one above the other. Bands 4 and 5 are used to create the NDVI image. The fractional vegetation cover (FVC) is determined by calculating the percentage of the total area covered by vegetation. The SW Algorithm uses the FVC picture to create the LSE picture. The LSE image quantifies the intrinsic properties of the surface of the Earth, namely its capacity to transform thermal or heat energy into radiant radiation. We require the emissivity values for soil and vegetation at bands (10 and 11) in order to calculate the LSE. After

obtaining the LSE pictures for bands (10 and 11) separately, we compute the average and difference of LSE. We provide distinct NDVI images for each class based on our classification into the soil and vegetation classes. The Landsat-9 also features two TIRS bands. For bands (10 and 11), we estimate brightness temperature (TB). In the thermal calibration, the TB converts the digital number values from the TIRS thermal raw bands (10 and 11) to the atmosphere's spectral peak (TOA). These SW parameter values, TB, mean LSE, LSE difference, and water vapor constant are used to calculate the LST. Conversely, MW uses LSE, wavelength of emitted light, and top-of-atmosphere brightness temperature to determine LST. Figs. 2 and 3 show a flowchart of the suggested SW and MW algorithm for LST calculation utilizing TIRS-2 bands (10 and 11) and OLI-2 sensor bands (2– 5).

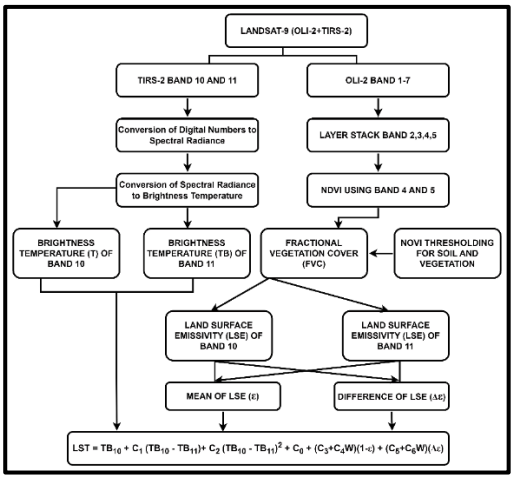

Fig.2 Flowchart of the SW.

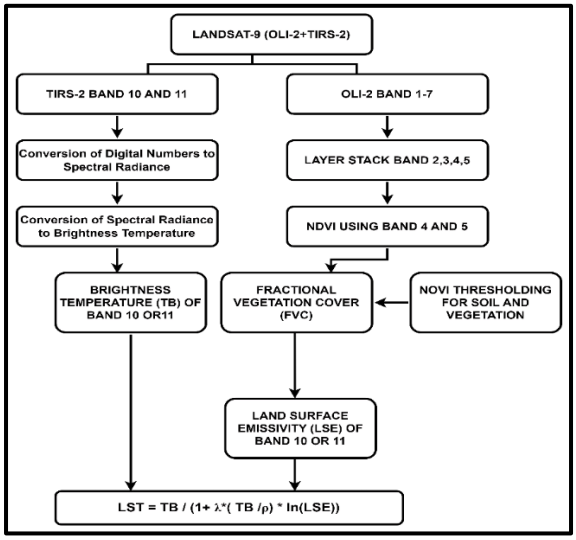

Fig.3 Flowchart of the MW.

3.1 Principle of Split-Window (SW) Algorithm

A novel technique called the SW algorithm takes into consideration how the environment absorbs two radiometric channels in the wavelength range of $(10-12.5\mu m)$ [35]. The original idea was to develop real-time patterns of surface temperature for water bodies, such as oceans, presuming that the outer layer is a black body. Subsequent research showed that the SW method effectively reduces the influence of low surface emittance on the calculation of sea surface temperature (SST). Additionally, the surface emittance consequence is cancelled within a tolerable scope of the total amount of the vapor of water in the atmosphere due to a little overestimation of the water vapor absorbed by the atmosphere [5, 36]. The SW approach performs an atmospheric influence cancelation by taking benefit of the differential absorption of atmospheric light in the two neighboring thermal infrared avenues, with peak values at $(11 \text{ and } 12\mu m)$. After that, it retrieves LST using nonlinear or linear combinations of temperatures of the brightness (TB)[30]. Since most sensors do not rely on precise knowledge about atmospheric profiles during data gathering, many split-window methods have been developed and optimized to consistently extract LST from diverse sensors[5]. The attempt to leverage a nonlinear structure of TB in the recovery of LST from the TIRS-2 of Landsat-9 led to the operationalization of an enhanced version of the modified SW method. Founded on the $(10-12\mu m)$ band range that TIRS-2 bands use, the suggested SW algorithm works on the principle of attenuating radiance for atmospheric assimilation, which corresponds to the disparity in brightness of synchronous dimensions at two distinct wavelengths that are each influenced by differing degrees of atmospheric assimilation [24, 37]. The mathematical formula for the SW algorithm for retrieval of the LST is given as follows[35, 38, 39]:

$$\mathbf{LST} = \mathbf{TB10} + \mathbf{C1}(\mathbf{TB10} - \mathbf{TB11}) + \mathbf{C2}(\mathbf{TB10} - \mathbf{TB11})\mathbf{2} + \mathbf{C0} + (\mathbf{C3} + \mathbf{C4W})(\mathbf{1} - \boldsymbol{\varepsilon}) + (\mathbf{C5} + \mathbf{C6W})(\boldsymbol{\Delta\varepsilon}) \quad \text{…… Eq.1}$$

In this case, W stands for total atmospheric water vapor content $(\mathrm{gm/cm^2})$, TB10, TB11 are the temperatures of the brightness of bands (10,11) in $(^{\circ}C)$, $\boldsymbol{\varepsilon}$ is the mean of the LSE of the TIRS-2bands (the emissivity of the mean), $\Delta\varepsilon$ is the difference of emissivity, and C0 to C6 are the SW coefficients to

be found from the simulated data. $\boldsymbol{\varepsilon = (\varepsilon 10 + \varepsilon 11)/2}$ is the mean emissivity, while $\boldsymbol{\Delta\varepsilon = (\varepsilon 11 - \varepsilon 10)}$ is the emissivity difference.

The sequential process for implementing the Split-Window algorithm is Namely:

Step 1:- Top of Atmosp here (TOA) Radiance.

The radiance of spectral of theTIRS-2 bands (10 and 11) and the OLI-2 sensor bands (2– 5) are independently evaluated using Eq. (2) to determine the TOA values and convert the DN to radiance[40]. The computing is executed utilizing the raster calculator in ArcGIS 10.8.

$$\boldsymbol{L\lambda = \left(\frac{L_{max} - L_{min}}{Qcal_{max} - Qcal_{min}}\right) Qcal + AL}$$

……..Eq.2

Where: -

Lλ : - TOA Spectral Radiance (W ($m^{-2} * sr^{-1} * \mu m^{-1}$)).

L_{max} : - Maximum Adiance (W ($m^{-2}*sr^{-1}*\mu m^{-1}$)).

L_{min} : - Minimum Radiance (W ($m^{-2}*sr^{-1}*\mu m^{-1}$)).

$Qcal_{max}$: - Maximum DN Value of pixels.

$Qcal_{min}$: - minimum DN Value of pixels.

Qcal : - Quantized and Calibrated Standard Product Pixel Values (DN).

AL : - Radiance Add Band (No.).

Step 2:- Conversion to Top of Atmosphere (TOA) Brightness Temperature.

Bands (10 and 11) are used to compute the temperature of brightness (TB). The electromagnetic irradiation that rises originating in the Earth's atmosphere is known as TB. After the TB was corrected, the Thermal Infrared Sensor (TIRS) underwent thermal calibration, which required translating the values of the thermal digital number of its raw thermal bands (10 and 11) into top-of-atmosphere (TOA) spectral radiation. The thermal infrared bands must be converted using the given metadata and the following equation in order to determine their brightness temperature (BT) [1].

$$\boldsymbol{TB = \frac{K_2}{\ln\left(\frac{K_1}{L_\lambda} + 1\right)} - 273.15}$$

……Eq.3

Where: - K_1 and K_2 :- The metadata file states the thermal constants for bands (10 and 11). L_λ = Denotes the highest point of spectral radiation in the Earth's atmosphere.

Step 3:- Normalized Differential Vegetation Index (NDVI).

An indicator that has been normalized for measuring vegetation is called the NDVI. In this instance, the NDVI was computed utilizing the collected optical bands (4 and 5), which are part of the OLI sensor band set. The NDVI scales its values from (-1 to $+1$). The normalized difference of the near infrared ($0.851 - 0.879\mu m$) and red ($0.636 - 0.673\mu m$) bands of a picture is used to calculate the NDVI for each pixel. The normalization formula that is applied is [1]:

$$\boldsymbol{NDVI = \frac{Band_5 - Band_4}{Band_5 + Band_4} = \frac{NIR - RED}{NIR + RED}}$$

……. Eq.4

Step 4:- The Fractional Vegetation Cover (FVC).

The application of Eq. 4 to the NDVI image produced in Step 3 yields the FVC image. It quantifies the amount of land surface area that is covered by vegetation. The SW approach used the FVC picture to obtain the LSE image. LSE is simply a measure of the capability of accommodating long-wave radiation in the electromagnetic spectrum of a given surface[41]. Some of the primary drivers affecting LSE are features relating to the target surface, for example, soil type, surface roughness, and vegetation cover of the area in question. The NDVI image is categorized into two separate classes: that of vegetation and soil[42]. The NDVI values for the soil and vegetation of the study area are calculated independently using ArcGIS 10.8. Eq. 5 is used to compute the image of FVC[5].

$$\boldsymbol{FVC = \frac{NDVI - NDVI_s}{NDVI_v - NDVI_s}}$$

…….. Eq.5

Where: - $NDVI_v$= NDVI of vegetation. $NDVI_s$= NDVI of soil.

Step 5:- Land Surface Emissivity (LSE).

Planck's equation of black body radiance is adjusted by the LSE, a scalar factor, to measure the brightness that is emitted. It shows how thermal energy can be transferred from the surface to the atmosphere [43]. An essential component of all LST retrieval techniques is LSE. Using the SW approach outlined in Eq. 6, the LSE picture is obtained originating in the FVC image obtained in step 4. The emissivity data for the vegetation and soil in bands (10 and 11) are necessary for the computation of LSE. [44]. For

each of the bands 10 and 11, two distinct LSE pictures are calculated. In comparison to land surfaces, the emissivity value of water bodies is significantly less changeable [43]. The NDVI can be utilized to assess the emissivity of various terrestrial surfaces in the $(10-12\mu m)$ range after accounting for this wavelength dependency. Table 2 provides these emissivity values [5].

$$\mathbf{LSE} = \boldsymbol{\varepsilon_s} \times (\mathbf{1} - \mathbf{FVC}) + \boldsymbol{\varepsilon_v} \times \mathbf{FVC} + \boldsymbol{C_\lambda}$$
…… Eq.6

In this case, $\boldsymbol{\varepsilon}_s$ & $\boldsymbol{\varepsilon}_v$:-The emissivities refer to the soil and vegetation, respectively. C_λ = represents the surface roughness ($C = 0$ for uniform and level surfaces) acquired as a constant value of 0.005.

Table 2. Values of the emissivity.

Emissivity	Band 10	Band 11
ε_s	0.971	0.977
ε_v	0.987	0.989

Then, to find the mean of the emissivity and the difference between the emissivity of Bands (10 and 11), as in Eqs. (7 and 8) [35].

Mean. of the LSE = $\boldsymbol{\varepsilon} = \frac{\mathbf{LSE_{10}} + \mathbf{LSE_{11}}}{\mathbf{2}}$
……Eq.7

Difference of the LSE = $\boldsymbol{\Delta\varepsilon} = \mathbf{LSE_{11}} - \mathbf{LSE_{10}}$
……...Eq.8

Step 6: Estimate Atmospheric Water Vapor (W).

When calculating LST using the S-W algorithm, we must assess the quantity of water vapor in the atmosphere (W). The W depends on temperature and relative humidity[45], according to the following mathematical relationship.

$$\mathbf{W} = \mathbf{h} \times \boldsymbol{\rho_w}$$ ……Eq.9

Where:- h:- Effective atmospheric height. ρ_w:- water vapor density (g/m^3).

To calculate the partial pressure of water vapor, we use the following relationship[46].

$$\mathbf{E} = \frac{\mathbf{E_s} \times \mathbf{H_r}}{\mathbf{100}}$$ …… Eq.10

Where:- E:- Partial water vapor pressure. H_r:- the relative humidity in percentage. E_s :- Saturated water vapor pressure.

The E_s depends on temperature (T) and is calculated using the Magnus-Tetten equation, which is the equation for calculating the E_s at a given temperature. They are widely used in hydrology and meteorology[47].

$$\mathbf{Es} = \mathbf{6.112} * \mathbf{exp}\left(\frac{\mathbf{17.67*T}}{\mathbf{T+243.5}}\right)$$
……...Eq.11

To estimate the density of water vapor, we use the following relationship[46].

$$\boldsymbol{\rho_w} = \frac{\mathbf{E}}{\mathbf{R \times T}}$$ …… Eq.12

Where:- R:- gas constant (461.5 J/kg*Kelvin). T:- Temperature in Kelvin.

Step 7: Calculate the LST

The final step is calculating the LST utilizing the brightness of the band's temperature (TB10, TB11) and the mean and difference LSE extracted from FVC and NDVI. The LST can be recovered using Eq. 1.

3.2 Principle of Mono-Window (MW) Algorithm

The MW algorithm underwent several stages to develop and reach the final version [48]. It was also developed by [49] and the work of [50] to obtain the final expression for the MW algorithm for LST retrieval, as in the equation below.

$$\mathbf{LST} = \mathbf{TB} / (\mathbf{1} + \boldsymbol{\lambda} * (\frac{\mathbf{TB}}{\boldsymbol{\rho}}) * \mathbf{ln}(\mathbf{LSE}))$$
……..Eq.13

Where:- LST:- land_ surface_ temperature (℃). TB :- Atmospheric radiance is measured at the top of the Earth's atmosphere, expressed as temperature. λ = wavelength of the radiated light (11.5μm). $\rho = (h / c\,\sigma)$ a constant, and its value is equal to $1.4388 * 10^{-2}$ mK. LSE = land surface emissivity calculated from Eq.6.

3.3 Assessment criteria

In this research, the RMSE and Bias equations were chosen to evaluate the performance of the algorithms adopted in this study. RMSE assesses the LST using the algorithm and the actual surface temperature measured at the site. Bias assesses the mean discrepancy between the surface temperature determined by the algorithm and the actual temperature registered at the site. The smaller the Bias, the closer the algorithm values are to the values

measured at the site. The following two equations give RMSE and Bias [51].

$$\mathbf{RMSE} = \sqrt{\frac{\sum_{i=1}^{n}(y_i - \hat{y}_i)^2}{n}} \quad \text{..... Eq.14}$$

Where: - y_i: -actual observed values. $\hat{y}_i$ = the predicted value. n = number of stations

$$\mathbf{Bias} = \frac{1}{n}\sum_{i=1}^{n}(\mathbf{T_{LST}} - \mathbf{T_{sit}}) \quad \text{..... Eq.15}$$

Where: - T_{LST} = LST by algorithm. T_{sit} = LST measured on site

4. Software Used and Data

In the present study, Landsat-9TIRS-2 bands (10 and 11) were exercised to rate the amount of TB and OLI-2 spectral bands $(2-5)$ were used to extract the vegetation index image of the Tigris River Basin. This study used The following software to process the Landsat-9 data: ENVI 5.3, ArcGIS 10.8, and SPSS 25. The thermal constants obtained from thermal constants were out from the used study area consisting of more than one scene (Table 3). The algorithms utilized in this study use metadata in the form of rescaling factors and thermal constants extracted from Landsat-9 L1TP bands as the main inputs for the LST estimation process.

Table 3. Metadata of Landsat-9 satellite image details of TIRS-2 and OLI-2[52].

Sensor	OLI-2	TIRS-2
Acquisition of Data	6/1/2024 and 4/4/2024	-
Elevation of Sun	30.16721693 and 55.75717574	-
Path/Row	167/38 and 168/37	-
Bands	9	2
Resolution	30 m	100 m
Radiance − Mult − Band − 10	-	0.00038
Radiance − Mult − Band − 11	-	0.000349
Radiance − Add − Band − 10	-	0.10000
Radiance − Add − Band − 11	-	0.10000
K1_Constant_Band_10	-	799.0284
K2_Constant_Band_10	-	1329.2405
K1_Constant_Band_11	-	475.6581
K2_Constant_Band_11	-	1198.3494

4. Results and Discussion

4.1 Retrieval LST by SW Algorithm

The NDVI images were generated using Eq. 4 and the ArcGIS 10.8 application by the data obtained with the help of the OLI2 sensor bands 4 and 5. Figure 4 presents the NDVI of the Tigris River in Wasit Governorate during the two study seasons. It is evident from these figures that the NDVI in the study area differs between (0.535743 to - 0.264062) in winter and (0.62717 to – 0.378722) in spring. High NDVI values closer to 1 indicate an area of healthy vegetation. The NDVI image was taken as the primary input image, which was then classified into some soil and vegetation categories. The average NDVI soil in winter was 0.13584, while in spring, it was 0.12422; the average NDVI of vegetation in winter was 0.39990, and in spring, it was found to be 0.502946. The NDVI value was used as information input to find the FVC using Eq.5; the raster maps acquired show the FVC during the two study seasons, as shown in Fig. 5.

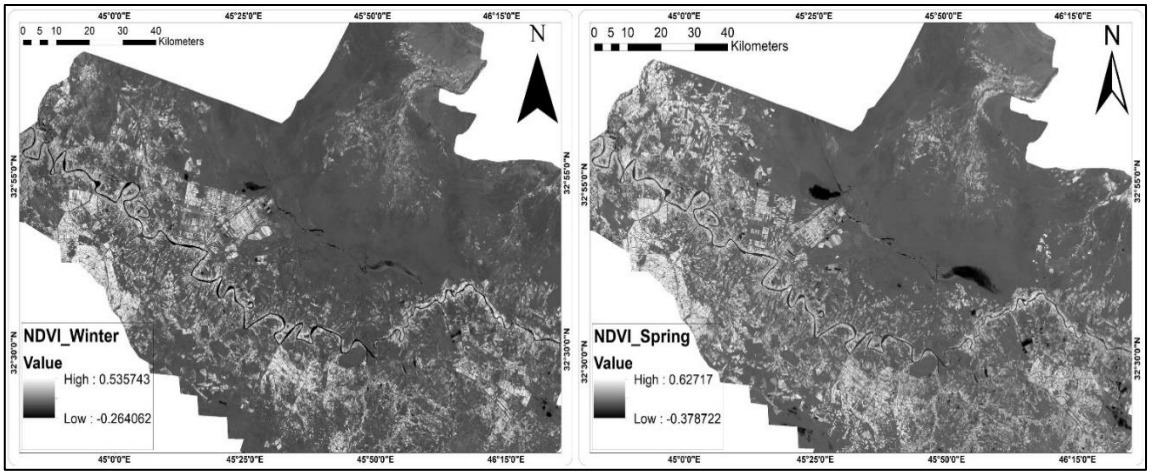

Fig. 4 NDVI image during the two study seasons.

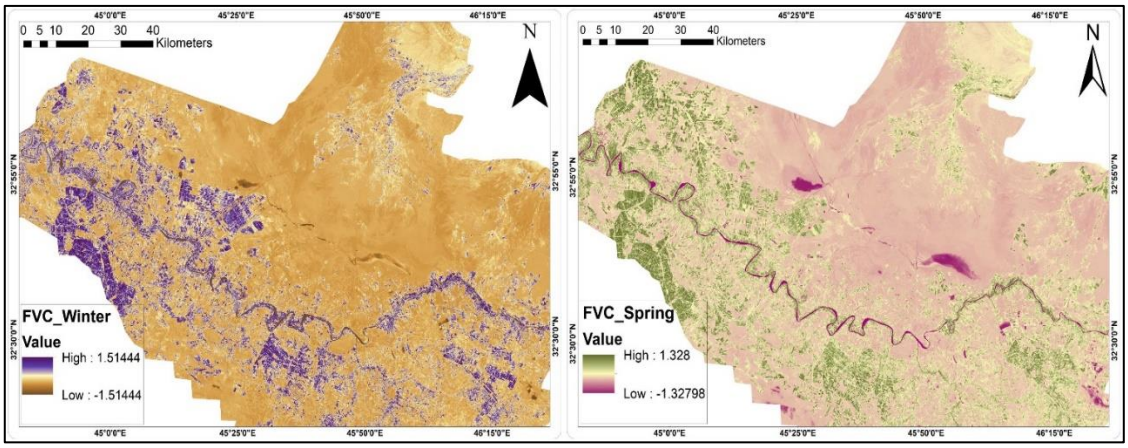

Fig. 5 FVC image during the two study seasons.

The Raster Calculator in ArcGIS 10.8 was used to execute the mathematical map calculations after LSE pictures for bands 10 and 11 for the two research seasons were acquired using Eq. 6. Figs. 6 and 7 display the raster maps that illustrate the mean LSE and difference for the bands 10 and 11 over the course of two seasons.

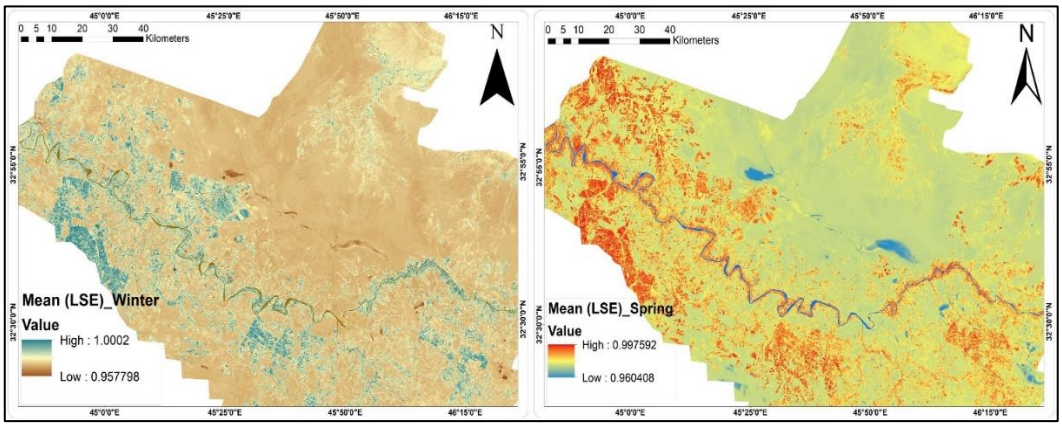

Fig. 6 Mean LSE image during the two study seasons.

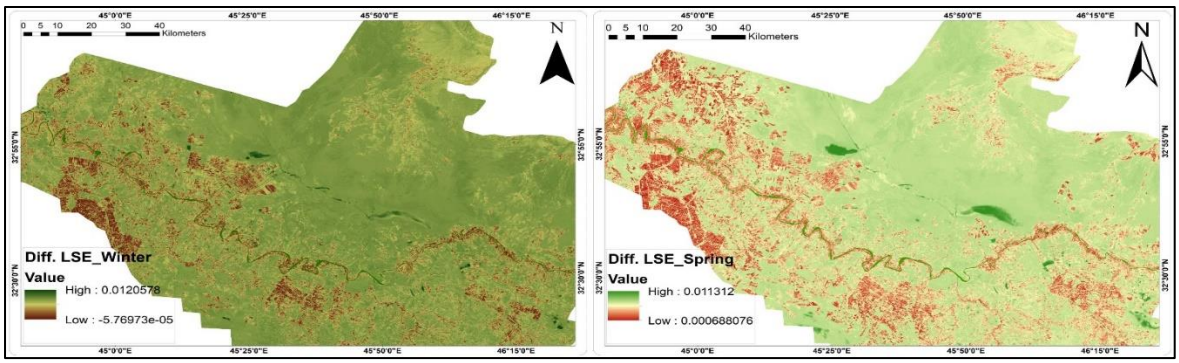

Fig. 7 Diff. LSE image during the two study seasons.

Furthermore, Eq.7 displays that the average LSE value for bands (10 and 11) ranges from (1.0002 to 0.957798) during January and (0.997592 to 0.960408) during April for the Tigris River Basin, as shown in Figure 6. Eq. 8 shows that the difference in LSE for the two thermal bands ranges from (0.0120578 to -0.00005769) in January and (0.011312 to 0.000688076) in April during the study period, as shown in Figure 7. From the NDVI values, we notice that this index is high in the areas close to the river, while the index values decrease in the regions far from the river. Also, in spring, the NDVI values increase in the study area, in contrast to winter, when the NDVI value decreases. The mean value of LSE in winter was (1.00023 to 0.951769) while it was (0.997592 to 0.960408) in spring. Therefore, the areas close to the river have higher LSE because they are agricultural areas, and the LSE decreases the further away from the river.

From Eq. 3, we estimated the temperature of the Tigris River using TRIS2 bands (10 and 11) at twelve stations and for two different seasons. Figures 8 and 9 display the calculated TB10 and TB11 for the study area for bands (10 and 11), respectively. Table 3 presents TB10 and TB11 data for both seasons. On 6 January, TB10 recorded the greatest temperature at ST1 (12.352℃) and the lowest temperature at ST8 (10.922℃). TB11 recorded Table 3 presents TB10 and TB11 data for both seasons. On 6 January, TB10 recorded the greatest temperature at ST1 (12.352℃) and the lowest temperature at ST8 (10.922℃). temperature in ST1 (14.720℃) and the lowest temperature in ST8 (12.845℃) in the study time. On 4 April, TB10 recorded the highest temperature (16.732℃) at ST10 and the lowest (14.583℃) at ST5. TB11 recorded the highest temperature (17.810℃) in ST10 and the lowest (15.956℃) in ST5 during the study time.

SW coefficients in Eq. 1, based on the non-linear multiple regression equation and using the SPSS 25 program, were found to be ($C0 = -0.268, C1 = 1.387, C2 = 0.183, C3 = 54.3, C4 = -2.238, C5 = -129.2,$ and $C6 = 16.4$) in this study. Regarding the water vapor in the atmosphere of the study area, relying on the region's temperature and humidity percentage and using Eqs. (9, 10, 11, and 12), it was found that W ($1.467\ g/cm^2$) in winter and ($1.256\ g/cm^2$) in spring.

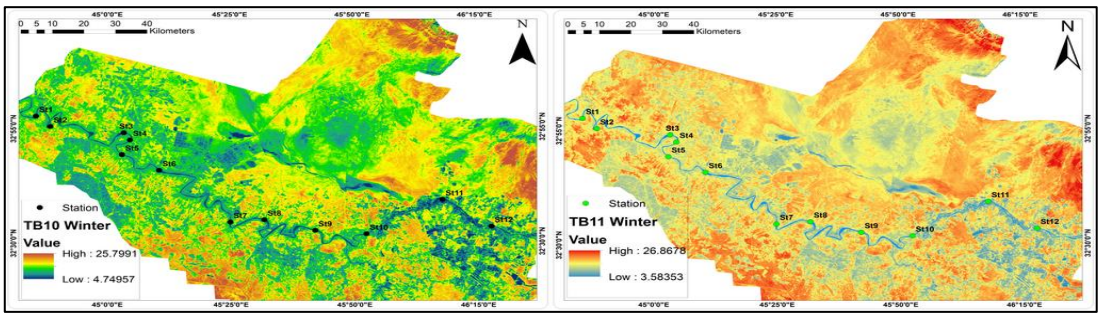

Fig. 8 Displays the TB10 and TB11 for the research area in Winter.

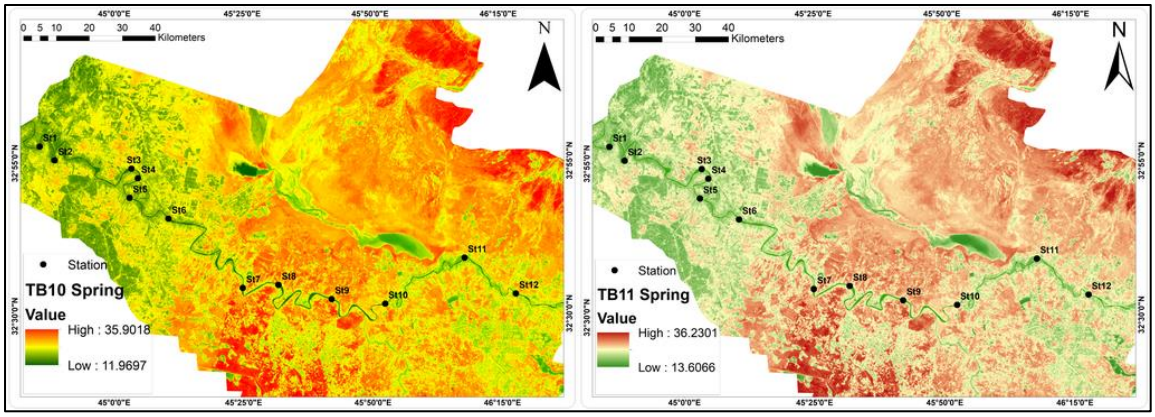

Fig. 9 Displays the TB10 and TB11 for the research area Spring.

Using Eq. 1 and utilizing all the variables and constants we have determined, we can calculate the value of LST using the suggested SW algorithm for the research area. Table 3 presents LST data for both seasons. Fig. 10 also shows the amount of LST during the study time. In this algorithm, in winter, the St5 recorded the lowest LST (9.275°C), whereas the St2 recorded the highest LST (10.651°C). In spring, the St5 station recorded the lowest LST (13.4141°C), while the St10 recorded the highest LST (15.8087°C).

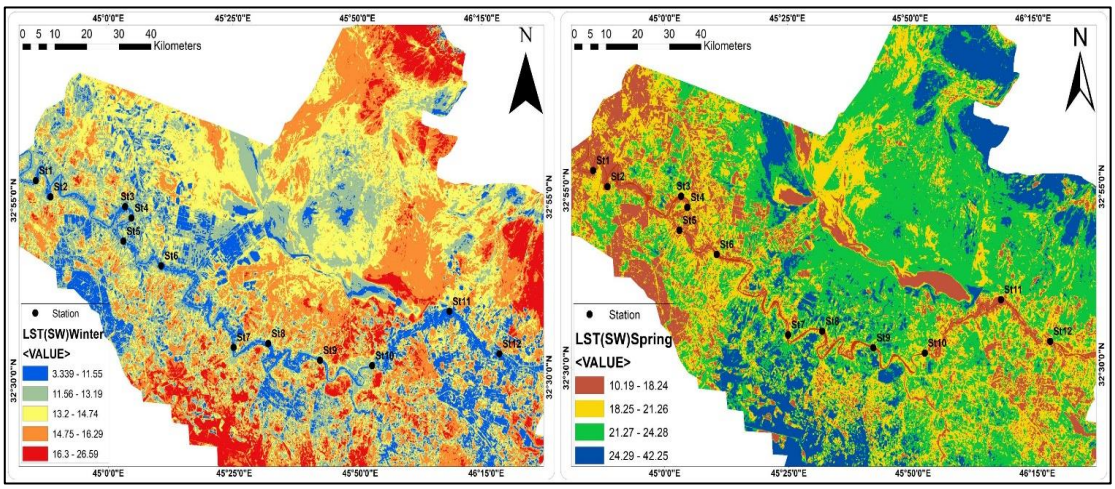

Fig. 10 Displays the LST retrieval from the SW algorithm for the two research seasons.

4.2 Retrieval LST by MW Algorithm

To find the LST for the MW algorithm, we use Eq.13, where the LST for both TIRS-2 bands (10 and 11) will be retrieved separately. Figure 11 displays the LST retrieval from the MW method. Table 3 shows the LST values for the MW algorithm in the study area and each season. It is essential to mention that because of the ability of band 11 to capture the water vapor signals intensely, it is inclined to severe variations in atmospheric profiles [53]. Thus, band 10 is employed to extract the LST using the MW method in this work. In this algorithm, in winter, the St8 recorded the lowest LST (10.926°C), whereas the St1 recorded the highest LST (12.357°C). In spring, the St5 station recorded the lowest LST (14.589°C), while the St10 recorded the highest LST (16.7434°C).

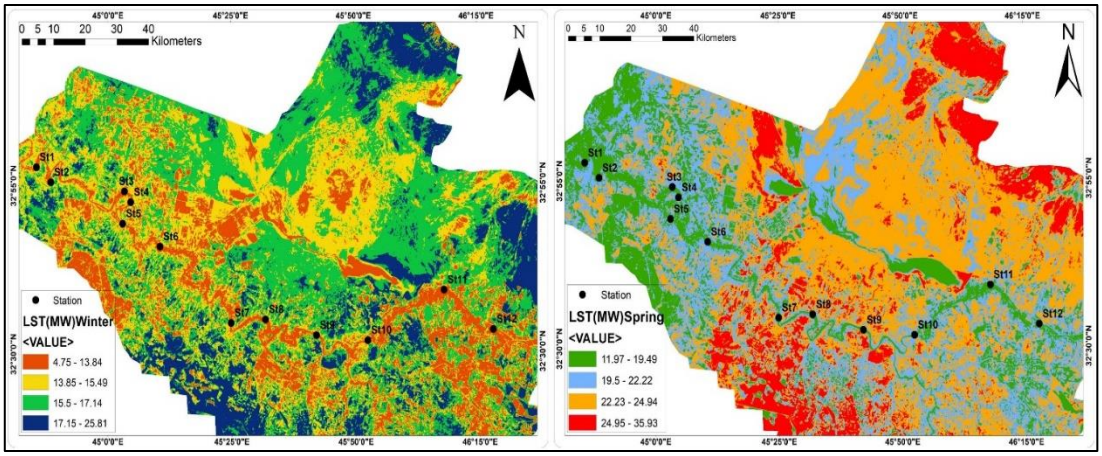

Fig. 11 Displays the LST retrieval from the MW algorithm for the two research seasons.

Table 3. The LST values for the MW and SW algorithm, as well as TB10 and TB11 in the study area and each season.

	6 January / Winter					4 April / Spring				
Station	**TB_{10} (°C)**	**TB_{11} (°C)**	**LST in Site (°C)**	**LST (MW) (°C)**	**LST (SW) (°C)**	**TB_{10} (°C)**	**TB_{11} (°C)**	**LST in Site (°C)**	**LST (MW) (°C)**	**LST (SW) (°C)**
St1	12.352	14.720	10.28	12.357	10.554	15.603	16.891	13.9	15.610	14.5029
St2	12.271	14.337	10.34	12.276	10.651	15.807	16.996	14	15.815	14.8070
St3	11.242	13.63	9.63	11.246	9.4507	15.515	16.598	14.1	15.523	14.6267
St4	12.075	14.334	9.74	12.0801	10.352	15.676	16.822	14.3	15.683	14.7226
St5	11.068	13.472	9.35	11.07	9.275	14.583	15.956	13.8	14.589	13.4141
St6	11.306	13.341	9.43	11.310	9.725	15.202	16.224	14.5	15.209	14.3563
St7	11.181	13.389	9.27	11.185	9.506	15.243	16.555	14.6	15.250	14.1047
St8	10.922	12.845	9.13	10.926	9.426	15.384	16.754	14.7	15.391	14.1995
St9	11.15	12.912	9.31	11.158	9.771	16.521	17.532	14.9	16.529	15.6460
St10	11.615	13.233	9.63	11.620	10.321	16.732	17.810	15.1	16.7434	15.8087
St11	11.287	12.849	9.19	11.300	10.082	16.433	17.428	15.4	16.446	15.6192

St12	11.766	13.552	9.82	11.911	10.393	16.598	17.676	15.5	16.604	15.7026
			RMSE	**1.9526**	**0.4684**			**RMSE**	**1.2864**	**0.5231**
			Bias	**1.9436**	**0.3660**			**Bias**	**1.2164**	**0.2259**

4.3. Comparison of Algorithms

LST of the selected region of the Tigris River has been calculated using the available data originating in Landsat-9TIRS 2. To verify the validity of the LST, air temperature is measured near the surface or through ground measurements. The results of this study are compared between the LST found by the MW algorithm, the LST found by the SW algorithm, and the actual temperature measured at the study site. Validation has shown that retrieved surface temperatures can differ by up to 5℃ contrasted to in situ measurements[5, 13]. We note from the results that the LST calculated by the WS algorithm recorded an RMSE of (0.4684℃) and a bias of (0.3660℃) in winter; this algorithm also recorded an RMSE of (0.5231℃) and bias of (0.2259℃) in the spring. While the LST measured by the MW algorithm recorded an RMSE of (1.9526℃) and a bias of (1.9436℃) in winter, this algorithm also recorded an RMSE of (1.2864℃) and a bias of (1.2164℃) in spring. From the results, we see that the SW algorithm has retrieved the temperature very close to the actual temperature measured at the site, and this is proven by RMSE and bias, where the reduced the RMSE value is than one, the closer the practical results are to the results calculated at the site (actual). While the bias, the higher the value is greater than one, the model may be very simple and cannot express the relationship between the temperature retrieved by the algorithm and the actual temperature correctly. In contrast, the case of a very low bias indicates that the model is very complex and does not express an ideal case for the model. Fig. 12 shows the in-situ calculated river surface temperature and the river surface temperature obtained using the SW and MW algorithms from Landsat- 9 on January 6 and April 4, 2024, at twelve different stations along the river. For the comparison, the air temperature was used, and the difference may be quite big due to the different resolutions of LANDSAT 9 for different bands. The thermal band was at 100 m, while the red and the nearinfrared bands were limited to 30 m. The variations could sometimes be considerable relying on the weather and other factors being experienced.

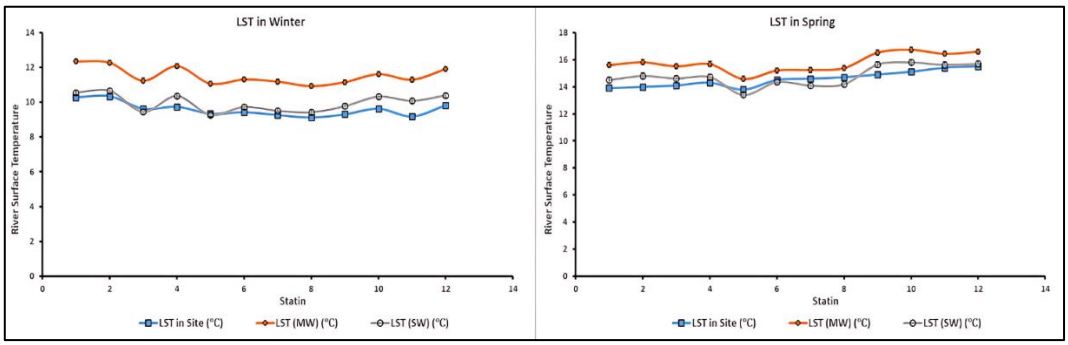

Fig. 12 Comparison between in situ temperature and the LST retrieval originating in the MW and SW algorithms for the two study seasons.

A comparison between the LST values calculated by applying the suggested SW algorithm and those estimated through the MW algorithm was made, and what has been observed is that the values are of a similar distribution. However, it is observed that the MW algorithm always produces LST values that are approximately two degrees different or less from the onsite LST. [13] discovered a discrepancy of 0.7 °C when retrieving LST compared to the average measurement of near-surface air temperature. An

algebraic test also reveals that should the temperature of LST(MW) go up by 1 °C, the temperature of LST(SW) would rise by approximately 0.905°C. The detailed regression analysis results for both LST techniques are shown in Fig. 13. The regression study between SW and MW algorithms for LST retrieval shows an R^2 value of 0.844 in winter and an R^2 value of 0.9819 in spring. Since the LST calculated from the studied data with the help of the SW algorithm is in good agreement with the LST estimated from the MW technique despite the difference between their temperatures and the actual site temperature of the river surface, it means that the transfer between them is linear, and no significant loss of accuracy is observed. The discrepancy in LST appreciation between the Split-Window (SW) and the Mono-Window (MW) methods can be ascribed to the difference in spectral bands and atmospheric water vapor levels utilized to retrieve LST.

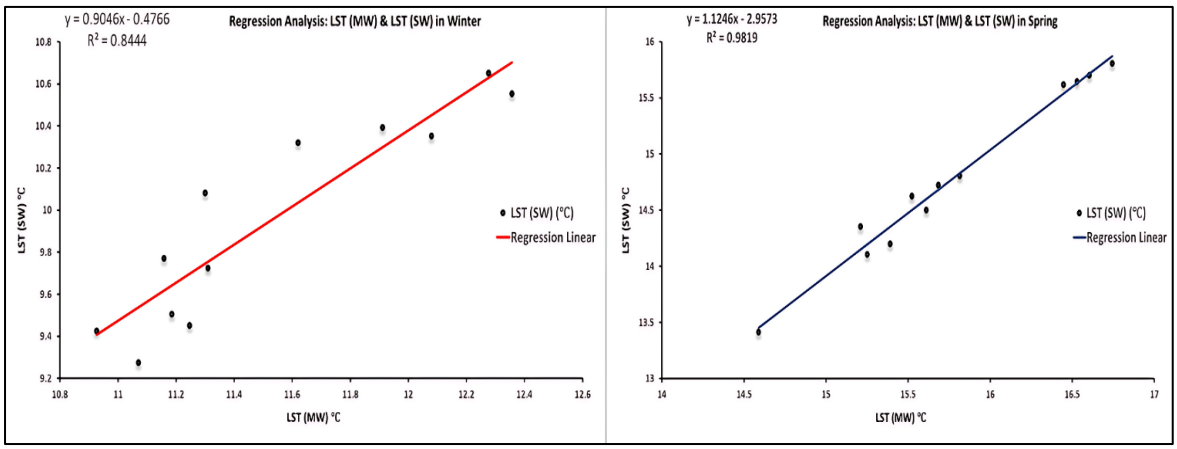

Fig. 13 The detailed regression analysis results for both LST techniques.

The variation in spectral bands and atmospheric water vapor levels utilized to obtain LST can be used as an explanation for the variance in LST appreciation between the SW and MW approaches. Bands 10 and 11 are the two bands used in the SW technique. The wavelengths at which these bands function are roughly 11 and 12 μm, respectively. In contrast, the MW method only employs band 10, which is located in the atmospheric window at a wavelength of roughly 11.5 μm. Furthermore, an accurate evaluation of the current conditions at the location is made possible by the SW algorithm, which depends on the location-specific atmospheric water vapor content. Nevertheless, the atmospheric water vapor quantity is not utilized in the MW approach. A major determinant of weather, water vapor content in the atmosphere, is particularly significant in regions with high surface temperatures. Emissionsivity and brightness temperature are computed by the SW technique using two spectral bands. The LST is subsequently obtained using these values along with the atmospheric water vapor content. In terms of delivering better results and precisely capturing field circumstances, the SW algorithm performs better than the MW method. On a variety of surfaces, this is more apparent.

5. Conclusions

The current research explores the viability of using remote sensing to measure surface temperatures in the Tigris River Basin in Wasit, where Landsat9 pictures were utilized to calculate LST using two methods (SW and MW). To estimate LST, the SW approach makes use of a dynamic mathematical tool. This algorithm depends on the amount of water vapor in the studyenvironment, the temperature of the brightness of the thermal bands from the TIRS2 sensor , and the LSE factor that is determined by FVC using the optical bands from the OLI2 sensor. Of all the operational techniques that are used to derive LST based on atmospheric factors, this one is the most often employed. LST retrieval at high spatial resolution greatly benefits from the presence of both bands, which increases the likelihood of notable gains. The LSE factor and one of the thermal bands from TIRES2 serve as the foundation for the

MW algorithm. The SW algorithm was assessed by contrasting its output with that of the MW method, as well as by utilizing in-situ (real) observations of the Tigris River's surface temperature in the Wasit Governorate. Both the SW and MW methodologies' LST values exhibit a similar order. In contrast to the SW algorithm and site temperatures, the MW algorithm predicts greater river surface temperature values. Based on the findings, RMSE, and Bias values, the SW algorithm demonstrated a significant convergence between its LST and the Tigris River surface LST. This is brought on by both the quantity of water vapor in the atmosphere and the application of TIRS2 bands. An R^2 value of 0.9819 in the spring and 0.844 in the winter is found in the regression analysis comparing the MW and SW algorithms for LST retrieval. Since there is no discernible loss of accuracy, the transfer between the LST estimated from the MW technique and the LST derived from the examined data using the SW algorithm is linear. The results show that LST can be recovered using the proposed SW approach. However, a thorough evaluation of the correctness of the SW algorithm in all seasons is still necessary. Furthermore, in order to evaluate the precision of the technique more effectively, more validation work for Land Surface Temperature (LST) must be conducted in the research area across a range of weather conditions and land cover types.

References

[1] M. M. Salih, O. Z. Jasim, K. I. Hassoon, and A. J. Abdalkadhum, "Land surface temperature retrieval from LANDSAT-8 thermal infrared sensor data and validation with infrared thermometer camera," International Journal of Engineering & Technology, vol. 7, no. 4.20, pp. 608-612, 2018.

[2] D. Philippus, A. Sytsma, A. Rust, and T. S. Hogue, "A machine learning model for estimating the temperature of small rivers using satellite-based spatial data," Remote Sensing of Environment, vol. 311, p. 114271, 2024.

[3] M. H. Tavares et al., "Derivation of consistent, continuous daily river temperature data series by combining remote sensing and water temperature models," Remote Sensing of Environment, vol. 241, p. 111721, 2020.

[4] P. K. Thakur and V. E. Gosavi, "Estimation of temporal land surface temperature using thermal remote sensing of Landsat-8 (OLI) and Landsat-7 (ETM+): A study in Sainj River Basin, Himachal Pradesh, India," Environ We Int J Sci Tech, vol. 13, no. 2018, pp. 29-45, 2018.

[5] G. Rongali, A. K. Keshari, A. K. Gosain, and R. Khosa, "Split-window algorithm for retrieval of land surface temperature using Landsat 8 thermal infrared data," Journal of Geovisualization and Spatial Analysis, vol. 2, pp. 1-19, 2018.

[6] T. Hu et al., "Monitoring agricultural drought in Australia using MTSAT-2 land surface temperature retrievals," Remote Sensing of Environment, vol. 236, p. 111419, 2020.

[7] S. A. Sahaar, J. D. Niemann, and A. Elhaddad, "Using regional characteristics to improve uncalibrated estimation of rootzone soil moisture from optical/thermal remote-sensing," Remote Sensing of Environment, vol. 273, p. 112982, 2022.

[8] Y. Bai, N. Bhattarai, K. Mallick, S. Zhang, T. Hu, and J. Zhang, "Thermally derived evapotranspiration from the Surface Temperature Initiated Closure (STIC) model improves cropland GPP estimates under dry conditions," Remote Sensing of Environment, vol. 271, p. 112901, 2022.

[9] L. Olivera-Guerra, C. Mattar, O. Merlin, C. Durán-Alarcón, A. Santamaría-Artigas, and R. Fuster, "An operational method for the disaggregation of land surface temperature to estimate actual evapotranspiration in the arid region of Chile," ISPRS Journal of Photogrammetry and Remote Sensing, vol. 128, pp. 170-181, 2017.

[10] T. Smith and B. Bookhagen, "Changes in seasonal snow water equivalent distribution in High Mountain Asia (1987 to 2009)," Science advances, vol. 4, no. 1, p. e1701550, 2018.

[11] Z. Zhang et al., "A review of satellite synthetic aperture radar interferometry applications in permafrost regions: Current status, challenges, and trends," IEEE Geoscience and Remote Sensing Magazine, vol. 10, no. 3, pp. 93-114, 2022.

[12] J. Townshend et al., "The 1 km resolution global data set: needs of the International

Geosphere Biosphere Programme," International Journal of Remote Sensing, vol. 15, no. 17, pp. 3417-3441, 1994.

[13] Z.-L. Li et al., "Satellite-derived land surface temperature: Current status and perspectives," Remote sensing of environment, vol. 131, pp. 14-37, 2013.

[14] T. Hu et al., "Continental-scale evaluation of three ECOSTRESS land surface temperature products over Europe and Africa: Temperature-based validation and cross-satellite comparison," Remote Sensing of Environment, vol. 282, p. 113296, 2022.

[15] X. Ye, R. Liu, J. Hui, and J. Zhu, "Land Surface Temperature estimation from Landsat-9 thermal infrared data using ensemble learning method considering the physical radiance transfer process," Land, vol. 12, no. 7, p. 1287, 2023.

[16] M. Wang et al., "Land surface temperature retrieval from Landsat 9 TIRS-2 data using radiance-based split-window algorithm," IEEE Journal of Selected Topics in Applied Earth Observations and Remote Sensing, vol. 16, pp. 1100-1112, 2022.

[17] B. Efremova et al., "Landsat 9 thermal infrared sensor 2 subsystem-level spectral test results," in IGARSS 2018-2018 IEEE International Geoscience and Remote Sensing Symposium, 2018: IEEE, pp. 8849-8852.

[18] M. Wang et al., "An efficient framework for producing Landsat-based land surface temperature data using Google Earth engine," IEEE Journal of selected Topics in applied earth observations and remote sensing, vol. 13, pp. 4689-4701, 2020.

[19] R. Niclòs et al., "Evaluation of Landsat-8 TIRS data recalibrations and land surface temperature split-window algorithms over a homogeneous crop area with different phenological land covers," ISPRS Journal of Photogrammetry and Remote Sensing, vol. 174, pp. 237-253, 2021.

[20] Q. Vanhellemont, "Combined land surface emissivity and temperature estimation from Landsat 8 OLI and TIRS," ISPRS Journal of Photogrammetry and Remote Sensing, vol. 166, pp. 390-402, 2020.

[21] A. Gerace, T. Kleynhans, R. Eon, and M. Montanaro, "Towards an operational, split window-derived surface temperature product for the thermal infrared sensors onboard Landsat 8 and 9," Remote Sensing, vol. 12, no. 2, p. 224, 2020.

[22] J. G. Masek et al., "Landsat 9: Empowering open science and applications through continuity," Remote Sensing of Environment, vol. 248, p. 111968, 2020.

[23] N. K. Malakar, G. C. Hulley, S. J. Hook, K. Laraby, M. Cook, and J. R. Schott, "An operational land surface temperature product for Landsat thermal data: Methodology and validation," IEEE Transactions on Geoscience and Remote Sensing, vol. 56, no. 10, pp. 5717-5735, 2018.

[24] L. M. McMillin, "Estimation of sea surface temperatures from two infrared window measurements with different absorption," Journal of geophysical research, vol. 80, no. 36, pp. 5113-5117, 1975.

[25] J. C. Price, "Land surface temperature measurements from the split window channels of the NOAA 7 Advanced Very High Resolution Radiometer," Journal of Geophysical Research: Atmospheres, vol. 89, no. D5, pp. 7231-7237, 1984.

[26] F. Becker and Z.-L. Li, "Towards a local split window method over land surfaces," Remote Sensing, vol. 11, no. 3, pp. 369-393, 1990.

[27] G. Franc and A. Cracknell, "Retrieval of land and sea surface temperature using NOAA-11 AVHRR· data in north-eastern Brazil," International Journal of Remote Sensing, vol. 15, no. 8, pp. 1695-1712, 1994.

[28] Z. Wan, "New refinements and validation of the collection-6 MODIS land-surface temperature/emissivity product," Remote sensing of Environment, vol. 140, pp. 36-45, 2014.

[29] Z. Qin, G. Dall'Olmo, A. Karnieli, and P. Berliner, "Derivation of split window algorithm and its sensitivity analysis for retrieving land surface temperature from NOAA-advanced very high resolution radiometer data," Journal of Geophysical Research: Atmospheres, vol. 106, no. D19, pp. 22655-22670, 2001.

[30] Z. Wan and J. Dozier, "A generalized split-window algorithm for retrieving land-surface temperature from space," IEEE Transactions

on geoscience and remote sensing, vol. 34, no. 4, pp. 892-905, 1996.

[31] D. Sun and R. Pinker, "Retrieval of surface temperature from the MSG-SEVIRI observations: Part I. Methodology," International Journal of Remote Sensing, vol. 28, no. 23, pp. 5255-5272, 2007.

[32] M. Wang et al., "A radiance-based split-window algorithm for land surface temperature retrieval: Theory and application to MODIS data," International journal of applied earth observation and geoinformation, vol. 76, pp. 204-217, 2019.

[33] D. Anandababu, B. Purushothaman, and B. S. Suresh, "Estimation of land surface temperature using Landsat 8 data," International Journal of Advance Research, vol. 4, no. 2, pp. 177-186, 2018.

[34] M. J. Issa, B. S. Al-Obaidi, and R. I. Muslim, "Evaluation of some trace elements pollution in sediments of the Tigris river in Wasit governorate, Iraq," Baghdad Science Journal, vol. 17, no. 1, pp. 9-22, 2020.

[35] F. Z. Rhziel, M. Lahraoua, and N. Raissouni, "Split-Window Algorithm for Land Surface Temperature Retrieval from Joint Polar-Orbiting Satellite System JPSS-2/NOAA-21," Environmental Sciences Proceedings, vol. 29, no. 1, p. 23, 2023.

[36] C. Ulivieri, M. Castronuovo, R. Francioni, and A. Cardillo, "A split window algorithm for estimating land surface temperature from satellites," Advances in Space Research, vol. 14, no. 3, pp. 59-65, 1994.

[37] V. Solanky, S. Singh, and S. Katiyar, "Land surface temperature estimation using remote sensing data," in Hydrologic Modeling: Select Proceedings of ICWEES-2016, 2018: Springer, pp. 343-351.

[38] D. Skoković et al., "Calibration and Validation of land surface temperature for Landsat8-TIRS sensor," Land product validation and evolution, 2014.

[39] J. A. Sobrino, Z.-L. Li, M.-P. Stoll, and F. Becker, "Multi-channel and multi-angle algorithms for estimating sea and land surface temperature with ATSR data," International Journal of Remote Sensing, vol. 17, no. 11, pp. 2089-2114, 1996.

[40] S. N. Reddy, B. Manikiam, and D. Jeevalakshmi, "Land surface temperature retrieval from LANDSAT data using emissivity estimation," International Journal of Applied Engineering Research, vol. 12, no. 20, pp. 9679-9687, 2017.

[41] J. A. Sobrino et al., "Land surface emissivity retrieval from different VNIR and TIR sensors," IEEE transactions on geoscience and remote sensing, vol. 46, no. 2, pp. 316-327, 2008.

[42] M. Stathopoulou and C. Cartalis, "Daytime urban heat islands from Landsat ETM+ and Corine land cover data: An application to major cities in Greece," Solar Energy, vol. 81, no. 3, pp. 358-368, 2007.

[43] U. Avdan and G. Jovanovska, "Algorithm for automated mapping of land surface temperature using LANDSAT 8 satellite data," Journal of sensors, vol. 2016, no. 1, p. 1480307, 2016.

[44] J. A. Sobrino, J. C. Jiménez-Muñoz, and L. Paolini, "Land surface temperature retrieval from LANDSAT TM 5," Remote Sensing of environment, vol. 90, no. 4, pp. 434-440, 2004.

[45] R. J. Ross and W. P. Elliott, "Tropospheric water vapor climatology and trends over North America: 1973–93," Journal of Climate, vol. 9, no. 12, pp. 3561-3574, 1996.

[46] R. Colman and B. J. Soden, "Water vapor and lapse rate feedbacks in the climate system," Reviews of Modern Physics, vol. 93, no. 4, p. 045002, 2021.

[47] O. A. Alduchov and R. E. Eskridge, "Improved Magnus form approximation of saturation vapor pressure," Journal of Applied Meteorology (1988-2005), pp. 601-609, 1996.

[48] Z. Qin, A. Karnieli, and P. Berliner, "A mono-window algorithm for retrieving land surface temperature from Landsat TM data and its application to the Israel-Egypt border region," International journal of remote sensing, vol. 22, no. 18, pp. 3719-3746, 2001.

[49] J. C. Jimenez-Munoz, J. A. Sobrino, D. Skoković, C. Mattar, and J. Cristobal, "Land surface temperature retrieval methods from Landsat-8 thermal infrared sensor data," IEEE Geoscience and remote sensing letters, vol. 11, no. 10, pp. 1840-1843, 2014.

[50] G. Rongali, A. K. Keshari, A. K. Gosain, and R. Khosa, "A mono-window algorithm for

land surface temperature estimation from Landsat 8 thermal infrared sensor data: a case study of the Beas River Basin, India," Pertanika J Sci Technol, vol. 26, no. 2, pp. 829-840, 2018.

[51] Y. Liu, Y. Wang, and G. Wang, "Land Surface Temperature Retrieval From GF5-01A Based on Split-Window Algorithm," The International Archives of the Photogrammetry, Remote Sensing and Spatial Information Sciences, vol. 48, pp. 431-436, 2024.

[52] USGS. "United States Geological Survey, Earth Explorer." https://earthexplorer.usgs.gov.

[53] C. Coll, V. Caselles, E. Valor, and R. Niclòs, "Comparison between different sources of atmospheric profiles for land surface temperature retrieval from single channel thermal infrared data," Remote Sensing of Environment, vol. 117, pp. 199-210, 2012.